Climate Dynamics (1990) 5:79–92

Climate Dynamics

A 3-D model for the Antarctic ice sheet: a sensitivity study on the glacial-interglacial contrast

Philippe Huybrechts

Geografisch Instituut, Vrije Universiteit Brussel, Pleinlaan 2, B-1050 Brussel, Belgium

Received November 29, 1989/Accepted August 29, 1990

Abstract. On the longer climatic time scales, changes in the elevation and extent of the Antarctic ice sheet have an important role in modulating global atmospheric and oceanographic processes, and contribute significantly to world-wide sea levels. In this paper, a 3-D time-dependent thermomechanical model for the entire ice sheet is presented, that is subsequently used to examine the effects of glacial-interglacial shifts in environmental boundary conditions on its geometry. The model takes into account a coupled ice shelf, grounding-line dynamics, basal sliding and isostatic bed adjustment and considers the fully coupled velocity and temperature fields. Ice flow is calculated on a fine mesh (40 km horizontal grid size and 10 layers in the vertical) for grounded and floating ice and a stress transition zone in between at the grounding line, where all stress components contribute in the effective stress in the flow law. There is free interaction between ice sheet and ice shelf, so that the entire geometry is internally generated. A simulation of the present ice sheet reveals that the model is able to yield realistic results. A series of sensitivity experiments are then performed, in which lower temperatures, reduced accumulation rates and lower global sea level stands are imposed, either singly or in combination. By comparing results of pairs of experiments, the effects of each of these environmental changes can be determined. In agreement with glacial-geological evidence, we found that the most pronounced changes show up in the West Antarctic ice sheet configuration. They appear to be essentially controlled by variations in eustatic sea level, whereas typical glacial-interglacial changes in temperature and ice deposition rates tend to balance one another. These findings support the hypothesis that the Antarctic ice sheet basically follows glacial episodes in the northern hemisphere by means of sea-level teleconnections. Grounding occurs more readily in the Weddell sea than in the Ross sea and long time scales appear to be involved: it may take up to 30–40 000 years for these continental shelf areas to become completely grounded after an initial stepwise perturbation in boundary conditions. According to these reconstructions, a steady state Antarctic ice sheet may contribute some 16 m to global sea level lowering at maximum glaciation.

Introduction

In recent years, a substantial body of observational evidence has become available, that documents important fluctuations in the configuration of the Antarctic ice sheet during the Pleistocene glacial cycles (Denton and Hughes 1981). The picture emerging from these glacial-geological data (exposed morainic deposits, glacial-marine sediments, etc.) seems to point in particular to drastic changes of the marine-based West Antarctic ice sheet (hereafter: WAIS). This ice sheet largely rests on bedrock well below sea level, even if isostatic depression were not accounted for, and appears to have basically oscillated between interior regions and a maximum state, where grounded ice may have extended all the way to the edge of the continental shelf. There seems to be a general agreement that this was also the case during the Wisconsin in the Weddell sea (Elverhøi 1981). However, there is currently still some doubt whether the shallow Ross sea was completely covered by grounded ice (Stuiver et al. 1981), or there was only a minor expansion (Drewry 1979), whereas in a recent discussion on the matter, Denton et al. (1989) seem to favour a more intermediate view. An important point here appear to be the long time-scales connected with the ice sheet evolution (Huybrechts 1990). The larger land-based East Antarctic ice sheet (EAIS), on the other hand, emerges as a comparably more stable feature, but even small fluctuations may have a major impact. Due to the huge amounts of ice involved here, a 1% increase in ice volume would lower global sea-level by 60 cm.

At the same time, more detailed field data on the present configuration of the ice sheet and on important boundary conditions have been compiled and mapped (Drewry 1983). In addition, stable isotope studies on the Vostok deep ice core have provided detailed infor-

mation on shifts in surface temperature (Jouzel et al. 1987) and accumulation rate (Yiou et al. 1985) during a full glacial-interglacial cycle. Chapell and Shackleton (1986) were able to derive a global sea-level curve from oxygen isotope records derived from foraminifera in deep-sea sediments.

In view of the availability of the information just described, dynamic 3-D modelling can play an important role in understanding the ice sheet for a variety of reasons. First, sensitivity experiments of the type 'all other things being equal' can help to disentangle the complex interaction of environmental controls (accumulation rate, ice surface temperature and sea level) on the behaviour of the ice sheet, and reveal the magnitude of the connected response time scales. Simulations of past Antarctic ice sheet configurations may then be of great interest in the light of reconstructions of global ice volume and sea levels during the Pleistocene ice ages. A detailed knowledge of the ice thickness distribution in space and time is also one of the boundary conditions for models of other components of the climatic system. If the model is able to simulate past ice sheet behaviour in agreement with geomorphological field evidence, it could then gain sufficient credibility to be used in predictions of future ice sheet changes, such as those associated with the expected greenhouse warming of the Earth's atmosphere. This paper aims at presenting such a 3-D model and to discuss results of sensitivity experiments on the glacial-interglacial contrast.

On glacial time scales, several mechanisms can be identified by which the Antarctic ice sheet reacts to changes in the global climate system. Ice temperature determines to a large extent the viscosity of ice, so that cooler basal shear layers will reduce deformation rates, leading to a thickening. Changes in ice deposition rates (ablation is negligible, especially in colder climates than today) are another factor and these also affect the amount of ice that is discharged into the ice shelf. Lower global sea level stands, induced by the glacial cycle on the continents of the northern hemisphere, reduce the thickness necessary for grounding in regions where the bed is below sea level. Changes in bed elevation due to isostatic bedrock adjustments area similar effect. This means that a successful model of the Antarctic ice sheet should contain a description of bedrock deformation and the fully-coupled ice flow and temperature fields over the entire ice domain. In particular, all factors affecting ice thickness at the grounding line, where a transition takes place from grounded ice flow to ice shelf flow, should be considered, because these ultimately control its position. Since an important part of the grounded ice is discharged through smaller-scale and relatively fast-flowing features such as ice streams and outlet glaciers, the numerical grid should be fine enough to capture the essential characteristics of the bedrock, in particular at the edge. In this respect also, the process of basal sliding has to be incorporated, as it might explain why relatively small surface slopes occur together with high velocities in West Antarctic ice streams (Budd et al. 1984).

During the past decade, several large-scale numerical models for the Antarctic ice sheet have been developed. On the one hand, the models of Herterich (1988), Verbitsky (1988) and Budd and Jenssen (1989) solve the full set of thermo-mechanical equations for 'shallow ice flow' on various spatial resolutions in 3-D space much along the lines originally drawn by Jenssen (1977). However, these models consider a stationary ice sheet geometry and do not allow for changes in the extent of the grounded ice and a coupled ice shelf. Another class of models deals explicitly with changes in the horizontal and vertical extent of the ice sheet, but consider vertically integrated flow and exclude thermodynamics (Budd and Smith 1982; Oerlemans 1982). In the latter model, a diagnostic relation for ice shelf thickness based on the degree of enclosure was included, although the need was recognized to consider ice shelves and grounding-line dynamics in a much more refined way.

As another step towards a more complete and detailed flow model of the Antarctic ice sheet, the present work deals with a time-dependent 3-D thermo-mechanical model, including a coupled ice shelf, grounding-line dynamics, basal sliding and isostatic bed adjustment. The primary difference between this model and those used in earlier studies is a rigorous treatment of the flow across the grounding line and in the floating ice shelves that enter the ocean, so that the position of the grounding zone during the calculations can be traced by means of a flotation criterion. Also, more efficient numerical techniques have been employed that allow for a much finer grid. The finite difference scheme is based upon the alternating-direction-implicit method and, in order to avoid boundary problems in the thermodynamic calculations, a new vertical coordinate scaled to local ice thickness, has been employed. The numerical grid has a horizontal spacing of 40 km and 10 layers in the vertical concentrated towards the base, where the shear concentrates. Part of the model builds on previous work, where a 2-D flowline version, excluding the possibility of changes in the horizontal domain, has been used to study thermomechanical response patterns with changing climate of the East Antarctic ice sheet (Huybrechts and Oerlemans 1988). We present a description of the equations and numerical techniques governing the 3-D model. The third section deals with the input data and the environmental forcing. A simulation of the present ice sheet follows in the fourth section. Results of a sensitivity study on the glacial-interglacial contrast, involving changes in global sea level, ice surface temperature and accumulation rate, are discussed in the following section. In an accompanying paper, (Huybrechts and Oerlemans this issue), we look at much shorter time scales, and present calculations on the response of the Antarctic ice sheet to future greenhouse warming.

Model description

The model formulated here essentially predicts ice thickness in space and time, as well as the three dimen-

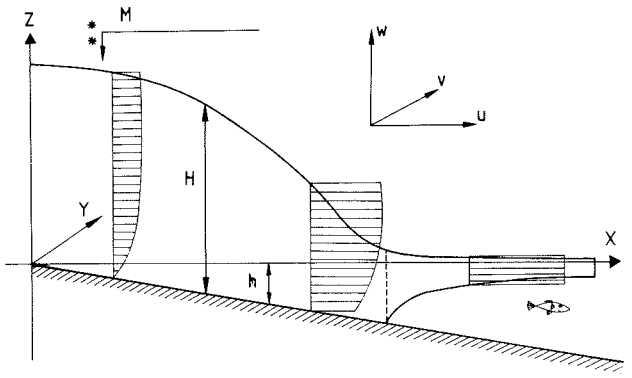

Fig. 1. Model geometry. The flow is calculated separately in the grounded ice region, the ice shelf and a stress transition zone in between. For explanation of variables, see text

sional flow and temperature distribution in response to specified atmospheric and environmental conditions. Defining a right-handed Cartesian coordinate system x, y, z, with the x, y plane parallel to the geoid and the z-axis pointing vertically upwards, the basic equation to be solved in the model is a continuity equation for ice thickness H:

$$\frac{\partial H}{\partial t} = -\nabla\cdot(\vec{v}H)+M \tag{1}$$

where $\vec{v}$ is the depth-averaged horizontal velocity vector, M the mass balance, t time (in years) and the ∇-operator is understood to be two-dimensional. This model geometry is shown in Fig. 1. In order to arrive at equations describing the velocity distribution, we start with the fundamental force balance acting on an element of ice:

$$\frac{\partial \tau_{xx}}{\partial x}+\frac{\partial \tau_{xy}}{\partial y}+\frac{\partial \tau_{xz}}{\partial z}=0 \tag{2}$$

$$\frac{\partial \tau_{yx}}{\partial x}+\frac{\partial \tau_{yy}}{\partial y}+\frac{\partial \tau_{yz}}{\partial z}=0 \tag{3}$$

$$\frac{\partial \tau_{zx}}{\partial x}+\frac{\partial \tau_{zy}}{\partial y}+\frac{\partial \tau_{zz}}{\partial z}=\rho g \tag{4}$$

and the flow law for polycrystalline ice, which is of Glen-type with exponent $n=3$ (Paterson 1981):

$$\dot{\varepsilon}_{ij}=A(T^*)\,\tau_*^2\,\tau'_{ij}$$
$$\text{and } \tau_*^2=\tau'^2_{xx}+\tau'^2_{yy}+\tau'_{xx}\tau'_{yy}+\tau^2_{xz}+\tau^2_{yz}+\tau^2_{xy} \tag{5}$$

In these expressions τ_{ij} are the stress tensor components, with $i\neq j$ the shear stresses, $i=j$ the normal stresses and an accent denoting stress deviators (defined as the full stress minus the hydrostatic component: $\tau'_{ii}=\tau_{ii}-(\tau_{xx}+\tau_{yy}+\tau_{zz})/3$). ρ is ice density [910 kgm^{-3}], assumed to be constant, and g the acceleration of gravity. $\dot{\varepsilon}_{ij}$ are strain rate components related to velocity gradients by definition ($\dot{\varepsilon}_{ij}=[\partial u_i/\partial x_j+\partial u_j/\partial x_i]/2$), τ^* the effective stress (where τ'_{zz} has been substituted employing the incompressibility condition: $\tau'_{xx}+\tau'_{yy}+\tau'_{zz}=0$) and $A(T^*)$ is a temperature-dependent flow law parameter, corrected for the dependence of the melting point on pressure: $T^*=T+8.7\,10^{-4}H$.

In ice, the vertical stress can generally be taken to equal the weight of the overlying ice ($\tau_{zz}(z)=-\rho g(H+h-z)$, with h bed elevation), allowing us to rewrite the stress equilibrium in a more convenient form for the analysis later. This is equivalent to the assumption that horizontal gradients in the vertical shear stresses are small compared to ρg in Eq. (4). After substituting for stress deviators and rearranging the terms, this gives:

$$\frac{\partial \tau_{xz}}{\partial z}=\rho g\frac{\partial(H+h)}{\partial x}-2\frac{\partial \tau'_{xx}}{\partial x}-\frac{\partial \tau'_{yy}}{\partial x}-\frac{\partial \tau_{xy}}{\partial y} \tag{6}$$

$$\frac{\partial \tau_{yz}}{\partial z}=\rho g\frac{\partial(H+h)}{\partial y}-2\frac{\partial \tau'_{yy}}{\partial y}-\frac{\partial \tau'_{xx}}{\partial y}-\frac{\partial \tau_{xy}}{\partial x} \tag{7}$$

These equations are in principle valid over the whole ice sheet domain, but are further simplified later by setting appropriate assumptions for the three separate flow regimes considered, namely grounded ice, floating ice and a transition zone in between at the grounding zone.

Grounded ice

In the case of grounded ice, variations in the longitudinal directions are small compared to the vertical (small aspect ratio), so that simplifications can be made according to the 'shallow ice approximation' (Hutter 1983). This implies the normal stress tensor to be isotropic, in effect ignoring longitudinal deviatoric stresses and lateral shearing. These are the usual assumptions, that are valid as long as gridpoint spacings are an order of magnitude larger than ice thickness and sufficiently small bedrock and surface slopes are considered (Nye 1969). These limitations are generally satisfied on a numerical grid, so that the stress balance is now between the horizontal shear stresses τ_{xz} and τ_{yz} and surface-slope induced pressure gradients. Ignoring atmospheric pressure, resulting expressions for the shear stress distribution can then be integrated to give:

$$\tau_{xz}(z)=-\rho g(H+h-z)\,\partial(H+h)/\partial x$$
$$\tau_{yz}(z)=-\rho g(H+h-z)\,\partial(H+h)/\partial y \tag{8}$$

Substituting these equations in the flow law (Eq. 5) and integrating the resulting equation with respect to the vertical then yields expressions for the horizontal velocity components:

$$\vec{v}(z)-\vec{v}(h)=-2(\rho g)^3[\nabla(H+h)\cdot\nabla(H+h)]$$
$$\nabla(H+h)\int_h^z A(T^*)(H+h-z)^3\,dz \tag{9}$$

with basal boundary condition $\vec{v}(h)$. Since the flow parameter $A(T^*)$ depends on temperature (and therefore on position), Eq. (9) has to be evaluated numerically, given the temperature distribution.

If the basal layers reach melting point, bottom water is formed and basal sliding may occur. Views on

how this should be modelled, however, differ widely. Here, we follow an analysis by Bindschadler (1983), and basal sliding is of Weertman-type (Weertman 1964), corrected for the effect of subglacial water pressure and restricted to regions that are at the pressure melting point:

$$\vec{v}(h) = -A_s(\rho g H)^3[\nabla(H+h)\cdot\nabla(H+h)]\nabla(H+h)/Z^* \quad (10)$$

where $A_s = 1.8\ 10^{-10}\ \mathrm{N^{-3}yr^{-1}m^7}$ and Z^* is the height above buoyancy:

$$Z^* = H + \rho_w(h - H_{sl})/\rho \quad (11)$$

where ρ_w is water density [1028 $\mathrm{kgm^{-3}}$] and H_{sl} sea level stand with respect to present conditions. This empirical relationship seemed to fit data from West Antarctic ice streams quite well and expresses the view that pressurized subglacial water reduces basal friction if the grounding line is approached, in turn leading to high sliding velocities.

A second integration with respect to the vertical then yields the mean horizontal ice mass flux:

$$\vec{v}H = \int_h^{H+h} \vec{v}(z)\,dz \quad (12)$$

where vertical motion, which occurs as a result of accumulation and vertical strain, is calculated from the incompressibility condition:

$$w(z) - w(h) = -\int_h^z \nabla\cdot\vec{v}(z)\,dz \quad (13)$$

with the kinematic boundary condition at the upper surface given by:

$$w(H+h) = \partial(H+h)/\partial t + \vec{v}(H+h)\cdot\nabla(H+h) - M \quad (14)$$

and M is positive in the case of accumulation. Equations (9) and (13) now fully describe the three-dimensional velocity field V, with the only limitation that $\vec{v}$ is not allowed to change direction with depth, that is solely determined by the local surface slope.

Ice shelf

In ice shelves, on the other hand, there is virtually no basal friction and shearing in horizontal planes, and a balance exists between the pressure gradient force arising from the surface slope and gradients in normal deviatoric stresses (that measure ice shelf stretching) and lateral shearing induced by side-walls and ice rises (Thomas 1973). This means that velocity and strain rate can be considered independently of z. With these simplifications in mind, equations describing the velocity distribution can be derived from Eqs. 6–7 substituting for the flow law (Eq. 5) and making use of the flow law in its second-order invariant form ($\dot{\varepsilon} = A(T^*)\tau^n$). After some algebraic manipulation, details of which are omitted for the sake of brevity, the following expressions can be shown to result [for a more rigorous derivation, the interested reader is referred to Herterich (1987), where a similar 2-D derivation is performed]:

$$2\frac{\partial}{\partial x}\left[f\frac{\partial u}{\partial x}\right] + \frac{\partial}{\partial x}\left[f\frac{\partial v}{\partial y}\right] + \frac{1}{2}\frac{\partial}{\partial y}f\left[\frac{\partial u}{\partial y} + \frac{\partial v}{\partial x}\right] = \rho g A(T^*)^{\frac{1}{3}}\frac{\partial(H+h)}{\partial x} \quad (a)$$

$$2\frac{\partial}{\partial y}\left[f\frac{\partial v}{\partial y}\right] + \frac{\partial}{\partial y}\left[f\frac{\partial u}{\partial x}\right] + \frac{1}{2}\frac{\partial}{\partial x}f\left[\frac{\partial u}{\partial y} + \frac{\partial v}{\partial x}\right] = \rho g A(T^*)^{\frac{1}{3}}\frac{\partial(H+h)}{\partial y} \quad (b)$$

$$\text{with } f = \left[\left(\frac{\partial u}{\partial x}\right)^2 + \left(\frac{\partial v}{\partial y}\right)^2 + \left(\frac{\partial u}{\partial x}\right)\left(\frac{\partial v}{\partial y}\right) + \left[\frac{1}{2}\left(\frac{\partial u}{\partial y} + \frac{\partial v}{\partial x}\right)\right]^2\right]^{\frac{-1}{3}} \quad (15)$$

Equations 15 (a–b) are a set of second-order partial differential equations of elliptic type, but nonlinear, and they are solved by point relaxation. In this way, an initial velocity distribution (u, v) is introduced and computed residuals are made zero locally in an iterative way until the maximum error on the grid is below a certain level, in this case 1 m/year. In general, once an initial velocity distribution has been obtained, convergence during the calculations is quite rapid, and only a few iterations proved to be necessary.

In the model, calving physics are not considered explicitly, and the ice shelf actually extends all the way to the edge of the numerical grid, but cutting off the ice shelf closer to the coast appeared not to influence the position of the grounding line. Boundary conditions at the seaward margin are then derived for unconfined, freely floating and uniform spreading (complete stress and strain-rate symmetry in the x- and y-directions) ice shelves, from the flow law and the condition that the total force on the ice shelf front must be balanced by the horizontal force exerted by the sea water:

$$\dot{\varepsilon}_{xx} = \partial u/\partial x = 3A(T^*)\tau'^3_{xx} \quad \dot{\varepsilon}_{yy} = \partial v/\partial y = 3A(T^*)\tau'^3_{yy}$$
$$\tau'_{xx} = \tau'_{yy} = \rho g H(1-\rho/\rho_w)/6$$
$$\partial u/\partial y + \partial v/\partial x = 0 = \dot{\varepsilon}_{xy} \quad (16)$$

At the grounding zone, boundary conditions are not velocity gradients, but follow from the vertically integrated velocity components.

Grounding zone

At the grounding zone, a transition takes place from shear-dominated flow to a situation where longitudinal stresses prevail, so that all stress components could be potentially important. Since the position of the grounding zone follows from a flotation criterion, all factors affecting changes in ice thickness should be carefully considered. These changes result from a delicate balance between local variations in surface mass balance and variations in the divergence of the mass flux, in turn depending on ice-shelf induced creep thinning and the amount of ice advected from upstream.

The role of longitudinal stresses in the flow of ice

sheets is a long-standing problem in glaciology and many papers have been devoted to it (Nye 1969; Shoemaker and Morland 1984; Alley and Whillans 1984; McMeeking and Johnson 1985; and many others). Of interest for numerical modelling are studies by Van der Veen (1985, 1987) and Herterich (1987), who addressed more specifically the flow at the grounding line in a 2-D flowline approach. The present 3-D approach incorporates some of their findings. As suggested by Herterich, the width of the stress transition zone is probably smaller than typical grid sizes in numerical models. Likewise, the grounding zone in the model consists of one gridpoint and is made up by all (grounded) gridpoints that border the floating ice region. Moreover, as shown by Van der Veen (1987), it is not really necessary to calculate longitudinal deviatoric stresses inside the ice sheet, since taking into account its value at the grounding line only, appears to change the ice sheet profile hardly at all. Also, neglecting the deviatoric stress gradients as a contribution to the shear stresses in the stress equilibrium (Eqs. 6–7), did not appear to be crucial to the model's outcome. This assumption may be somewhat doubtful, in particular in fast-flowing outlet glaciers and ice streams, where basal sliding becomes important and longitudinal stretching may support part of the weight (e.g. McMeeking and Johnson 1985). In spite of this, one could simply argue that this is probably the only thing to do, since it would otherwise imply complicated and time-consuming stress integrations along the x- and y-axes respectively. On the other hand, in a recent detailed calculation on the stress distribution near the grounding zone of Byrd Glacier (an outlet of the East Antarctic ice sheet), Whillans et al. (1989) also found a close correlation between the driving stress and basal drag. This indicates, that as far as large-scale numerical models are concerned, the ice sheet approximation may still be valid, so that shear stresses follow from the usual equations (Eq. 8). Other assumptions in Van der Veen's analysis are also implied here, such as replacing the deviatoric stresses by their vertical mean, since information on their vertical profile is lacking.

In view of this, the vertically integrated mass flux at the grounding line (that is of final interest) can also be found by integrating expressions for the shear strain rates $\dot{\varepsilon}_{xz}$ and $\dot{\varepsilon}_{yz}$ twice along the vertical, however incorporating all stress components in the effective stress in the flow law:

$$\begin{aligned}\vec{v}H = &-2(\rho g)^3 [\nabla(H+h)\cdot\nabla(H+h)]\nabla(H+h)\\ &\int_h^{H+h}\int_h^z A(H+h-z)^3\,dz\,dz\\ &-2\rho g[\overline{\tau'^2_{xx}}+\overline{\tau'^2_{yy}}+\overline{\tau'_{xx}}\,\overline{\tau'_{yy}}+\overline{\tau^2_{xy}}]\\ &\nabla(H+h)\int_h^{H+h}\int_h^z A(T^*)(H+h-z)\,dz+\vec{v}(h)H \qquad (17)\end{aligned}$$

where $\overline{\tau'_{xx}}$, $\overline{\tau'_{yy}}$, $\overline{\tau'_{xy}}$ in the transition zone follow by invoking the constitutive relation (Eq. 5). Integrating expression for $\dot{\varepsilon}_{xx}$, $\dot{\varepsilon}_{yy}$, $\dot{\varepsilon}_{xy}$ along the vertical and dividing by ice thickness to obtain vertical mean values yields:

$$\begin{aligned}&\frac{1}{H}\int_h^{H+h}\dot{\varepsilon}_{ij}\,dz=\frac{1}{H}\int_h^{H+h}[A(T^*)\cdot(\tau'^2_{xx}+\tau'^2_{yy}\\ &+\tau'_{xx}\tau'_{yy}+\tau^2_{xy}+\tau^2_{xz}+\tau^2_{yz})\cdot\tau'_{ij}]\,dz\\ &\text{for } \dot{\varepsilon}_{xx},\ \dot{\varepsilon}_{yy},\ \dot{\varepsilon}_{xy} \qquad (18)\end{aligned}$$

Since τ'_{xz}, τ'_{yz} follow from Eq. 8 and all strain rates can be calculated from the velocities that result on the grid, this represents a (non-linear) system of three equations in the three unknowns ($\overline{\tau'_{xx}}$, $\overline{\tau'_{yy}}$, $\overline{\tau'_{xy}}$) that is solved by an iterative method. About 5 iterations turned out to be necessary to reach a stable solution.

The main effect of treating the transition zone in this way is that the ice is apparently softened there (the depth-averaged deviatoric longitudinal stresses may be up to 3 times larger than shear stresses), so that lower shear stresses are needed to produce the same ice flux. Also, this treatment fully couples ice shelf flow to the inland flow regime. Since longitudinal stresses reflect the dynamic state of the ice shelf as well, in this way the deformational velocity at the grounding line (and indirectly also the basal sliding velocity through changes in the ice sheet geometry) is able to react to changes in the ice shelf geometry. For instance, restraining forces in the ice shelf that inhibit free spreading will thicken the ice at the grounding line, while unrestricted flow will cause thinning (wherafter driving stress is reduced, which causes thickening, so there is a counteracting effect). The whole coupling scheme seems to work well, as it allows the grounding line to move in both directions in response to environmental change.

Thermodynamics

In order to close the set of equations specifying ice deformation, the temperature distribution needs to be known simultaneously in order to adjust the ice stiffness parameter. This is necessary, since $A(T^*)$ changes by three orders of magnitude for the temperature range encountered in polar ice sheets (−50° C–0° C; Paterson 1981). Laboratory experiments suggest an Arrhenius relationship:

$$A(T^*)=m\cdot a\exp\left\{\frac{-Q}{RT^*}\right\} \qquad (19)$$

where $a=1.14\,10^{-5}\,\mathrm{Pa}^{-3}\,\mathrm{year}^{-1}$ and $Q=60$ kJmol^{-1} for $T^*<263.15$ K, $a=5.4710^{10}\,\mathrm{Pa}^{-3}\,\mathrm{year}^{-1}$ and $Q=139$ kJmol^{-1} for $T^*\geq 263.15$ K, R the gas constant [8.314 Jmol^{-1}K^{-1}] and T^* [K] pressure-corrected absolute ice temperature. The enhancement factor m serves a 'tuning purpose', in this way implicitly including the softening effects due to impurity content and crystal fabric. In the model runs discussed here, its value is set at 5 for grounded ice and 1 for the ice shelf.

The temperature distribution within the ice sheet is obtained from the thermodynamic equation:

$$\frac{\partial T}{\partial t}=\frac{k}{\rho c_p}\nabla^2 T-\vec{V}\cdot\nabla T+\frac{\Phi}{\rho c_p} \qquad (20)$$

Here T is temperature, and k and c_p (temperature dependent) thermal conductivity [$\mathrm{Jm^{-1}K^{-1}yr^{-1}}$] and specific heat capacity [$\mathrm{Jkg^{-1}K^{-1}}$] respectively. In this equation, heat transfer is considered to result from vertical diffusion (first term), three-dimensional advection (second term), and deformational layer heating $\Phi = 2\dot{\varepsilon}_{xz}\tau_{xz} + 2\dot{\varepsilon}_{yz}\tau_{yz}$. Boundary conditions follow from the mean annual air temperature at the upper surface. At the base, geothermal heating and dissipation due to sliding are incorporated in the basal temperature gradient. A value of 54.6 $\mathrm{mW/m^2}$ is taken for the geothermal heat flux (Sclater et al. 1980). In the ice shelf, the effects of basal melting and/or basal accretion and of spatially varying density and ice stiffness were ignored. Instead, a steady state linear vertical temperature distribution, with a surface temperature of $-18°\,\mathrm{C}$ (representing present day ice shelf conditions and allowed to vary with climatic change) and a fixed basal temperature of $-2°\,\mathrm{C}$ was assumed to exist within the ice shelves. The flow parameter is then taken to represent mean ice shelf temperature conditions.

Bed adjustment

Finally, bed adjustments are calculated with an earth deformation model that consists of a viscous fluid asthenosphere enclosed by a uniform, thin and elastic lithospheric shell. The time-dependent response of the underlying substratum is described by a diffusion equation for bedrock elevation h (e.g. Oerlemans and Van der Veen 1984, Chap. 7):

$$\frac{\partial h}{\partial t} = D_a \nabla^2 (h - h_0 + w) \tag{21}$$

where $D_a = 0.5\ 10^8\,\mathrm{m^2\,yr^{-1}}$ is the asthenosphere diffusivity, h_0 the undisturbed bed topography and w the deflection. The rigidity of the lithosphere is also taken into account, as this gives rise to deviations from *local* isostatic equilibrium (order of magnitude: 50 m). The deflection follows from (Brotchie and Sylvester 1969; Turcotte and Schubert 1983):

$$D\nabla^4 w = q - \rho_m g w \tag{22}$$
$$q = \rho_i g H \quad \text{if} \quad -\rho_i/\rho_w H + H_{sl} \leq h$$
$$q = \rho_w g (H_{sl} - h) \quad \text{if} \quad -\rho_i/\rho_w H + H_{sl} > h$$

where D is lithospheric flexural rigidity [10^{25} Nm] and ρ_m mantle rock density [3300 $\mathrm{kgm^{-3}}$]. The right-hand side gives the applied load q minus the upward buoyancy force arising when the lithosphere bends downwards into the astenosphere; the left-hand side represents the internal forces opposing lithospheric flexure. Equation (22) is solved by Kelvin functions of zero order (Brotchie and Sylvester 1969). Since bending of a rigid plate is a linear process, isostatic displacements on gridpoints due to varying ice and water loading have been superimposed in a square with sides of 800 km.

Numerical scheme

Since it is rather inconvenient to integrate the thermodynamic equation in the computational phase on a grid fixed in space, as the upper and lower ice boundaries will generally not coincide with grid-points, a new vertical coordinate ζ, scaled to local ice thickness, has been introduced. Following Jenssen (1977), this stretched dimensionless vertical coordinate is defined by:

$$\zeta = (H + h - z)/H \tag{23}$$

such that $\zeta = 0$ at the surface and $\zeta = 1$ at the base. The way all the relevant equations are transformed into this non-orthogonal system can be found in Huybrechts and Oerlemans (1988). In this approach, velocity and temperature fields are computed at levels of constant ζ (the layer interfaces). In the present model, the vertical domain was subdivided into ten layers concentrated towards the base, with an uppermost layer thickness of $\Delta\zeta = 0.15$ and a lowermost grid spacing of $\Delta\zeta = 0.02$, which proved to be sufficient to capture the essential characteristics of the model variables.

In order to solve the continuity equation numerically, we opted for a finite-difference approach (Huybrechts 1986). A staggered grid in space was employed, so that mass fluxes are calculated in between grid points. Smoothing in this way turns out to keep the integration stable. The resulting finite-difference equations are usually quite readily solved by an explicit integration scheme. However, such a scheme has the considerable drawback that in order to preserve stability, small time steps necessarily have to be taken. Alternatively, the alternating-direction-implicit (ADI) method turned out to work satisfactorily (Mitchell and Griffiths 1980). This is a two-step method involving the solution of sets of equations along lines parallel to the x- and y-axes at the first and second step respectively. Although not unconditionally stable, due to the non-linearity of the flow law, this scheme allows time steps to be taken an order of magnitude larger than an explicit approach. The resulting tri-diagonal systems are then easily solved by Gaussian elimination.

A comparable approach was applied to the solution of the thermodynamic equation. Here, the terms involving ζ-derivatives were made implicit, leading once more to a set of tri-diagonal equations that had to be solved at every gridpoint. However, a note about the horizontal advective terms is in order here, because replacing the derivatives by central differences turned out to generate oscillations in the solution. This problem is usually circumvented in diffusion-convection equations with a high Peclet number (i.e., a constant proportional to the ratio of advective velocity and diffusivity) by introducing an artificial horizontal diffusion process (e.g. Mitchell and Griffiths 1980). We use an "upwind" differencing scheme. Although this scheme can be shown to introduce an artificial horizontal diffusivity equal to $v\Delta r/2$, where v is the velocity and Δr the gridspacing, such an approach keeps the integration stable and influences results only marginally, as in most cases, the

associated artificial heat transfer turns out to be an order of magnitude smaller than the horizontal heat-advection term. In the model, spatial resolution is 40 km, allowing time steps up to 40 years. The complete model is run on a CRAY-2 computer, and takes around 18 min CPU time for a 10000 year integration.

Data and environmental forcing

Model inputs are bed topography, surface temperature, mass balance, thermal parameters and an initial state (which may be a thin slab of ice of equal thickness). The external forcing is made up by prescribing eustatic sea level stand and a uniformly spread background temperature change, that drives changes both in the accumulation and surface temperature distribution. The model then essentially outputs the time-dependent three-dimensional ice sheet geometry, and the fully coupled velocity and temperature fields. Bedrock elevation, surface elevation and ice thickness data for the present ice sheet have been interpolated from an original 20 km-digitalisation by the Australian group (Budd et al. 1984) of the Drewry (1983) map folio series and have been locally complemented beneath ice shelf areas with data from bathymetric charts (GEBCO, Canadian Hydrographic Service) and more recent sources (Herrod 1986). A contoured representation of the resulting initial bed topography is shown in Fig. 2. The square grid, laid out over a stereographic projection with standard parallel at 71° S, is centred at the pole and comprises a 141 × 141 grid point matrix. With 11 layers in the vertical, this adds up to a total of over 200000 gridpoints. The undisturbed bedrock heights, needed in the bed adjustment calculations, have been reconstructed assuming present isostatic equilibrium.

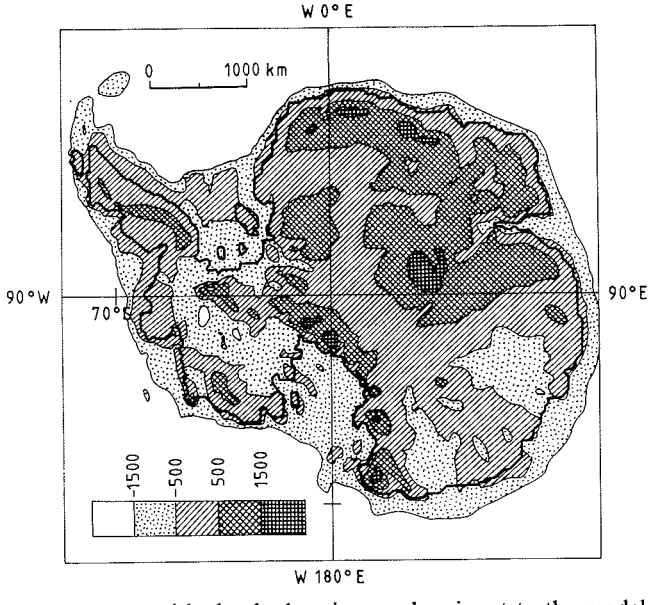

Fig. 2. Measured bedrock elevation used as input to the model. The *thick line* is the present grounding line. Units are in m above contemporary sea level

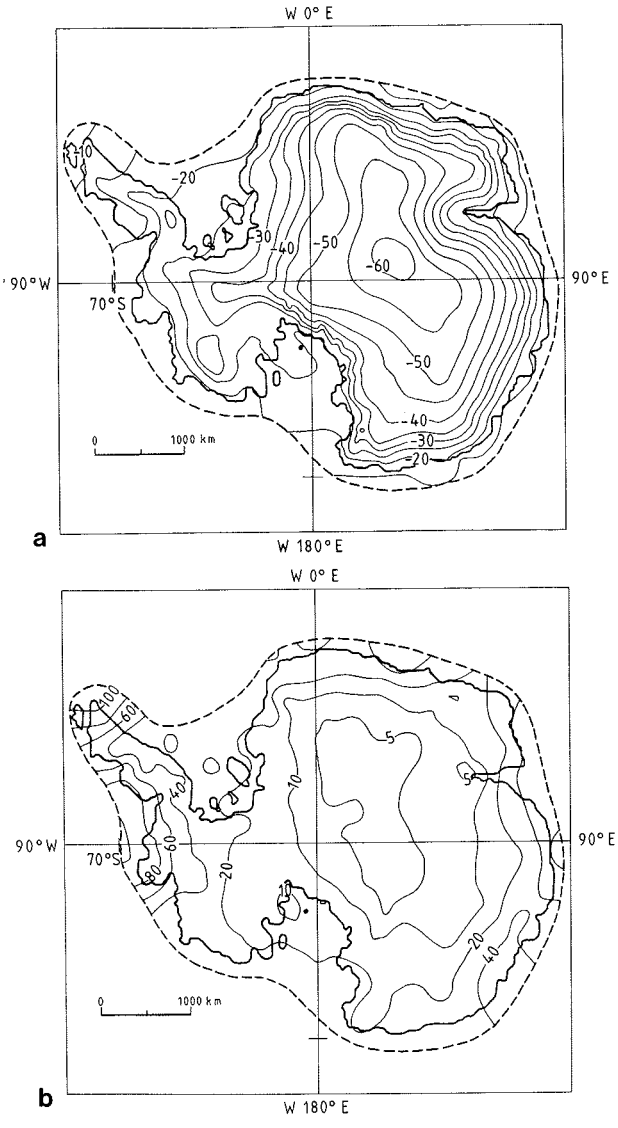

Fig. 3 A, B. Interpolated climatic data sets, to be perturbed in the experiments. **A:** 10 m-ice temperature (°C). **B:** accumulation rate (cm/y of ice). Data outside the *stippled* line are not shown, as they do not influence the model outcome

This may introduce an error, because uplift following the last glacial-interglacial transition some 15000 years ago is probably still in progress (Greishar and Bentley 1980), but a sound alternative is not readily available.

Basic climatic data sets for the 10 m-ice temperature and surface accumulation rate have been obtained by computer interpolation on original measurements (approximately a thousand points as compiled at Scott Polar Research Institute, Cambridge) and are shown in Fig. 3. The gridded temperature data are then perturbed in response to changes in background temperature (assumed uniform over the ice sheet) and local changes in surface elevation according to an atmospheric lapse rate of 5.1° C/1000 m below the 1500 m contour and 14.3° C/1000 m above the inland plateau. These values are suggested by a multiple regression analysis performed on the raw data by Fortuin and Oerlemans (1990).

Changes in surface temperature also serve to calculate accumulation rates in different climates. As first noticed by Robin (1977), the precipitation rate over Antarctica appears to be strongly governed by the water-vapour saturation-pressure above the surface inversion layer, with a relation similar to the Clausius-Clapeyron equation. It is this argument that was employed to help in dating the Vostok ice core (Lorius et al. 1985), and is also used here to alter the basic accumulation distribution in response to changes in temperature. This approach in estimating the past precipitation pattern seemed to agree well with accumulation rates deduced from cosmogenic ^{10}Be (Yiou et al. 1985). Furthermore, after a careful reexamination of the Byrd, Dome C and Vostok ice core chronologies, Jouzel et al. (1989) concluded that the vapour pressure argument can probably be extended all over the ice sheet. So, the temperature of formation of precipitation T_f is assumed to be close to the temperature prevailing above the surface inversion layer, leading to (Jouzel and Merlivat 1984):

$$T_f[\mathrm{K}] = 0.67\, T_s[\mathrm{K}] + 88.9 \qquad (24)$$

Then, as in Lorius et al. (1985), the accumulation rate for any perturbed climatic state is obtained from the product of its reference (present) value, times the ratio of the derivatives of the water-vapour saturation-pressure over a plane surface of ice for the reference and the perturbed state:

$$M[T_f(t)] = M[T_f(\text{present})] \cdot \exp\left\{22.47\left[\frac{T_0}{T_f(\text{present})} - \frac{T_0}{T_f(t)}\right]\right\} \cdot \left\{\frac{T_f(\text{present})}{T_f(t)}\right\}^2 \qquad (25)$$

$T_0 = 273.16$ K is the triple point of water. For surface temperatures prevailing over Antarctica, resulting accumulation rates are typically 50–60% of their Holocene values for a 10° C temperature decrease. This approach implies that the precipitation pattern is not allowed to follow changes in ice sheet geometry or a different pattern of high and low pressure areas and the associated storm tracks. This may be questionnable, in particular at the ice sheet margin, although it should be mentioned here that in a multiple regression study on these accumulation data, Fortuin and Oerlemans (1990) did not find significant correlations with such factors as distance to open water and surface slope (related to orographic effects). Moreover, as mentioned before, there are strong indications to suggest that the temperature of the inversion layer is the really relevant variable, also in past climates. This is attributed to relatively simple meteorological conditions over the Antarctic ice sheet (Jouzel et al. 1989).

Modelling the present state

Before embarking on the sensitivity study, a reference state has to be defined. This is necessary since it is unlikely that the input data are in full internal equilibrium with the model physics and it is completed in several steps. First, the coupled velocity and temperature fields are run forward in time for 100 000 years in a diagnostic way (thus keeping ice thickness and the grounding line position fixed) until an approximate steady solution settles down. This long time scale needed to reach stationary fields appears to be mainly due to thermo-mechanical effects and the low accumulation rates involved (Huybrechts and Oerlemans 1988). In a subsequent stage, the position of the grounding line is still prescribed, but ice thickness is allowed to relax to steady state. The result is shown in Fig. 4, where in addition a comparison is made with the observed field. Modelled ice thicknesses then appear to be within 5–10% or so of these, which is certainly acceptable. Some-

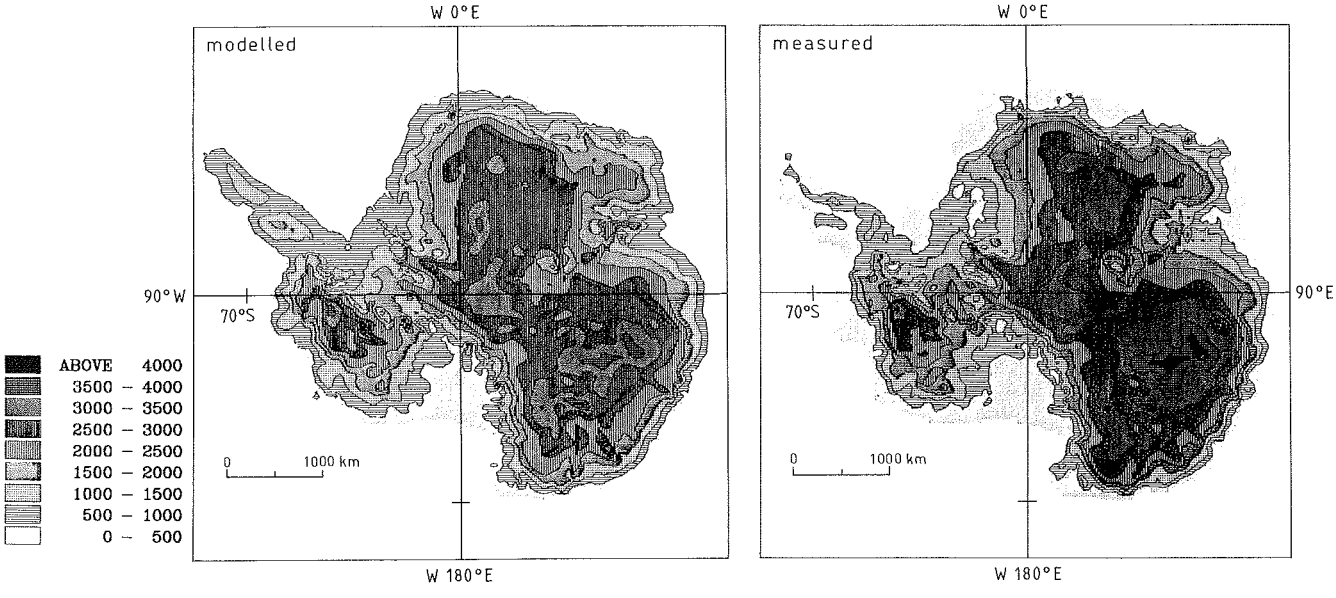

Fig. 4. A comparison between modelled and measured ice thicknesses (m). In this run, the position of the grounding line is still prescribed, but ice thickness is a free variable

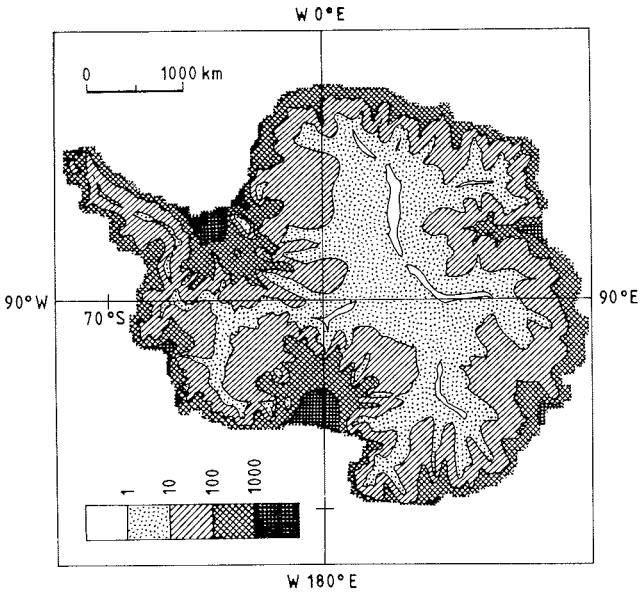

Fig. 5. Calculated velocity field (m/y) in the interglacial reference run, prescribed grounding line

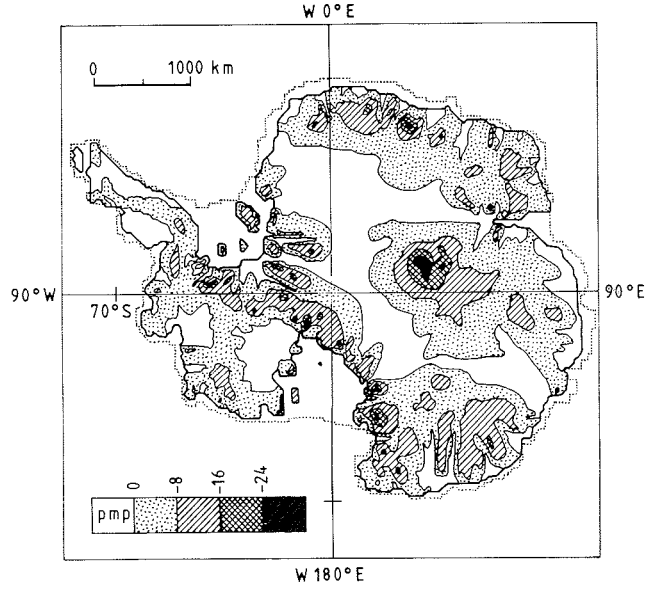

Fig. 6. Calculated basal temperature distribution (in °C) relative to the pressure melting point (pmp) for present conditions and prescribed grounding line

what larger deviations are found in the Pine Island and Thwaites Glacier catchment areas (approx. 90° W, WAIS) and upstream of the Shackleton Range in Dronning Maud Land (30–40° W, EAIS). However, this does not necessarily have to mean that the model is in error. Alternatively, insufficient bedrock data coverage in these areas and/or the fact that the ice sheet is just not in steady state there, could both play a role.

The associated (depth-averaged) velocity and basal temperature fields (relative to pressure melting) are displayed in Figs. 5–6 and provide an additional check on global model performance. As far as can be judged from available data, the velocity field looks quite reasonable, with very low velocities over central East Antarctica, typically around 200 m/y at the grounding line and up to 1500 m/y along central portions of the three major floating ice regions, the Ronne-Filchner, Amery and Ross ice shelves. These ice shelf velocities seem to agree rather well with observations (Robin et al. 1983; Thomas et al. 1984; Budd et al. 1982), although they tend to be somewhat higher at the ice shelf front. This may be due to the neglect of basal melting in the mass balance of the ice shelf. Although ice streams and outlet glaciers (discharging an important fraction of the ice mass into the ocean) do not enter the calcualtions explicitly, they show up distinctly and major outlet glaciers are characterized with velocities up to 500 m/y (Fig. 5). This is essentially a consequence of the fine grid in use. Basal areas at pressure melting then appear to be a dominant feature over most of the Antarctic Peninsula and are also widespread in West Antarctica. In East Antarctica, basal melting is confined to the thick interior regions (due to the insulating effect of ice) and the fast flowing regions at the margin (Fig. 6). This temperature field can be reconciled with independent evidence for temperate ice from radio-echo sounding, where sub-ice lakes in central areas have been found to obscure reflections (Oswald and Robin 1973). The coolest basal layers are found above the Gamburtsev Mountains, where the ice is relatively thin (1500–2000 m) and along the fringing mountain ranges. Here, both thin ice and cold ice advecton from above play a role.

Finally, also variations in the extent of the grounded ice sheet come into play and the grounding line is allowed to move freely according to hydrostatic equilibrium. The resulting ice sheet geometry after another 100000 years of model calculations is shown in Fig. 7 (1), and will serve as the interglacial reference run. Somewhat larger deviations from the present observed state include thicker ice in the Antarctic Peninsula (mainly due to poor bedrock data below the present ice shelf areas), a slight recession at the seaward edge of the most overdeepened EAIS outlet glaciers (Totten, Ninnis and Mertz Glaciers) and complete grounding of Henry ice rise in the Ronne ice shelf. However, considering the complexity of the model and the fact that the complete geometry is *internally generated,* the resulting configuration is certainly acceptable, and the model seems capable of reproducing the most important characteristics of the ice sheet.

Sensitivity study

In order to examine how environmental factors combine to produce the glacial extent, as documented in the geological record, the model has been subjected to shifts in accumulation rate, surface temperature and eustatic sea level of typical glacial-interglacial magnitude. These are a 10° C uniformly distributed temperature drop over the entire ice sheet, the associated reduction in surface deposition rates (calculated relative to

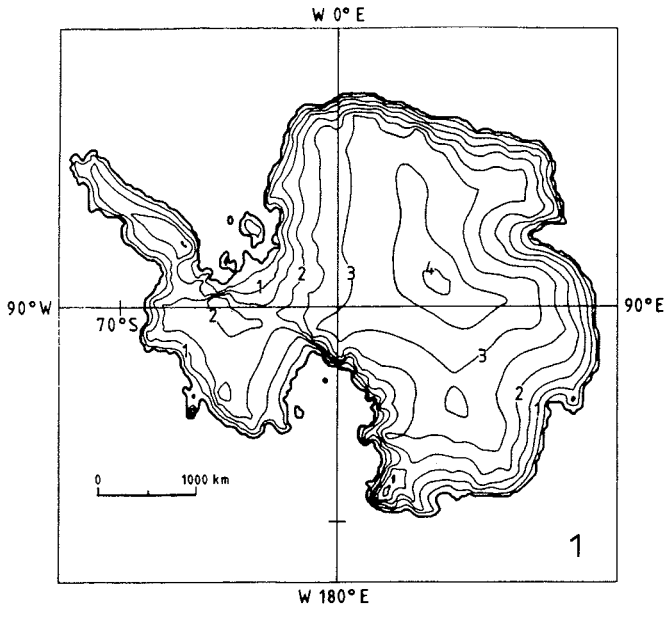
W 0° E
90° W
90° E
70° S
W 180° E
0 1000 km
1

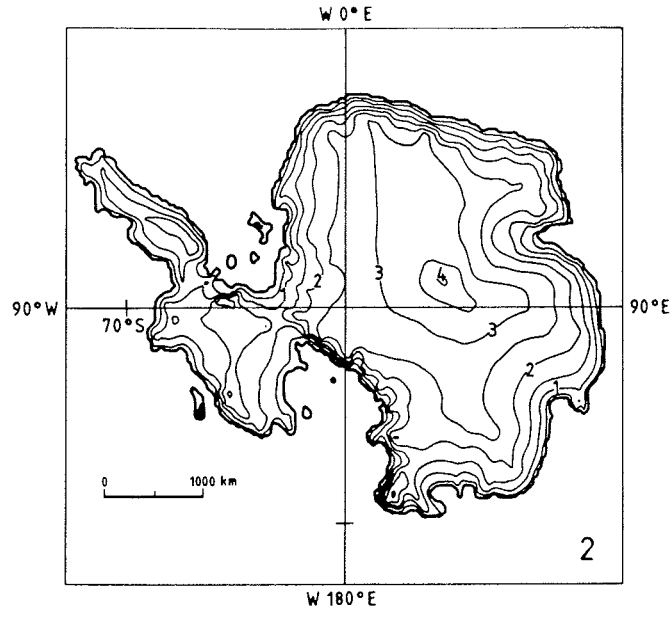
W 0° E
90° W
90° E
70° S
W 180° E
0 1000 km
2

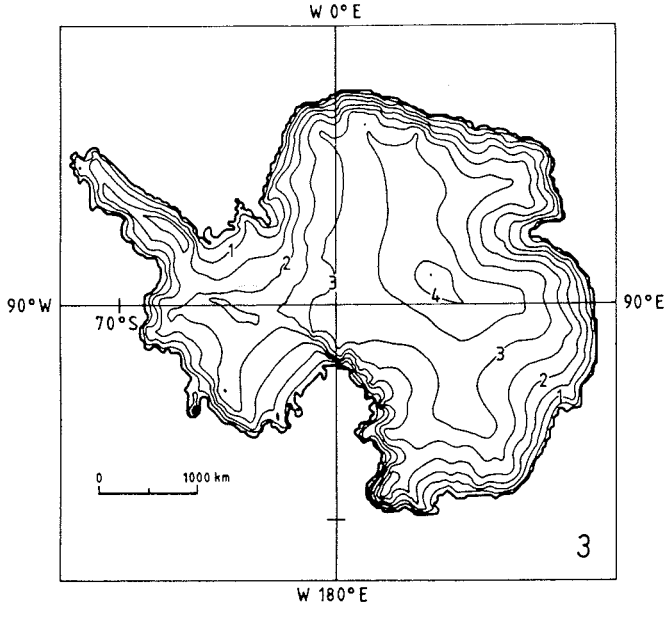
W 0° E
90° W
90° E
70° S
W 180° E
0 1000 km
3

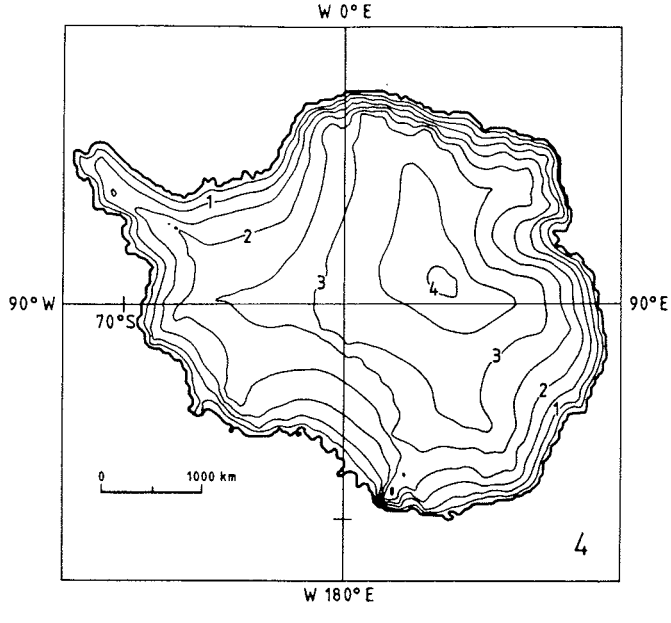
W 0° E
90° W
90° E
70° S
W 180° E
0 1000 km
4

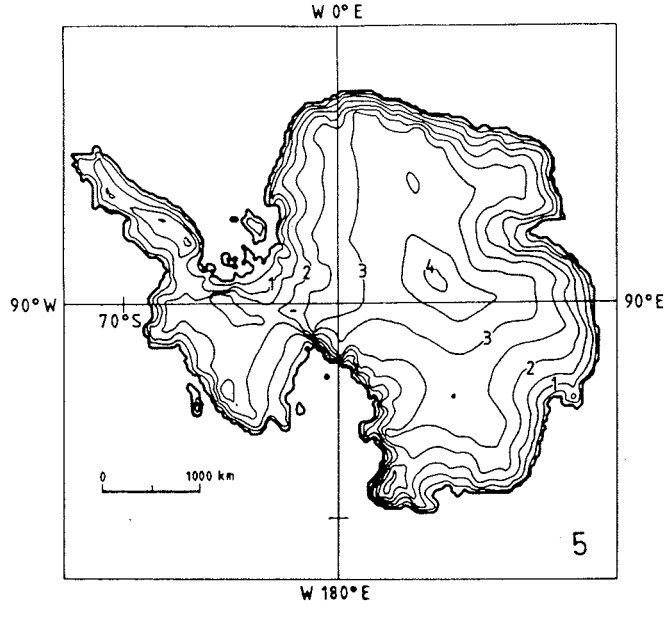
W 0° E
90° W
90° E
70° S
W 180° E
0 1000 km
5

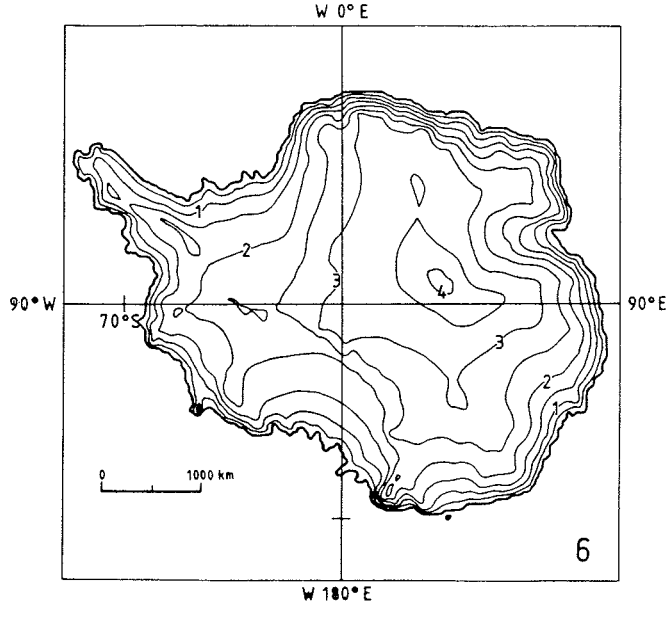
W 0° E
90° W
90° E
70° S
W 180° E
0 1000 km
6

the saturation water vapour pressure of the air circulating above the surface inversion layer) and a global sea level depression of 130 m. This strategy should allow insight to be gained in their relative importance and the connected response time scales. Another potentially important external forcing, namely melting beneath ice shelves, has been disregarded, simply because its present distribution is not known very well, let alone the potential effect of a modified sub-shelf circulation during glacial times. However, since the interest is in colder climates than today, it is not considered likely that bottom melting could have played a major role.

Six experiments were considered, in which each of the above mentioned factors are involved, either singly or in combination. In these experiments, sudden stepwise changes in boundary conditions were applied and the model ran 100000 years forward in time, starting from the present relaxed model ice sheet. Resulting geometries are displayed in Fig. 7.

Lowering accumulation rate to glacial levels (that are about 50% of Holocene values) then results in a thinning of grounded ice by several hundred meters (Fig. 7, 2). This effect is further enhanced by grounding line retreat in the WAIS, but although the grounding line enters progressively deeper water, it appears that a new equilibrium can still be established between ice thickness and water depth and there is no collapse. An opposite effect can be seen when lower surface temperatures are imposed, that eventually reduce deformation rates in basal layers (Fig. 7, 3). In this case, ice volume increases substantially over East Antarctica and an important part of the Ronne ice shelf runs aground on the shallow seabed, resulting in a remarkable advancing of the grounding line. As these effects appear to be of comparable magnitude, but of opposite sign, it comes as no surprise to find the ice sheet geometry rather unchanged, when both climatic conditions now operate together (Fig. 7, 5). From this, it is also clear that Antarctic ice sheet fluctuations cannot be studied without taking into account thermodynamics, because a colder climate will not only influence the surface mass balance, but thermal conditions at depth as well, due to a complicated interaction between changes in cold ice advection, thermal conduction and strain heating (dissipation).

As is also evident from Fig. 7, by far the most decisive environmental factor is eustatic sea level: lowering sea level by only 130 m (Fig. 7, 4) appears to be enough to initiate complete grounding over the shallow continental shelf areas. The effect is particularly drastic over the WAIS, whereas seaward changes of the EAIS remain rather limited. This is a direct consequence of the subglacial bed topography. Imposing full glacial conditions (Fig. 7, 6) then reduces ice thickness somewhat, but the extent of the ice sheet appears to be primarily governed by fluctuations in sea level. Comparing Fig. 7, 6 with Fig. 7, 1 (the reference run) demonstrates that surface elevations over the EAIS have not really changed much, whereas the thickening in its western counterpart is much more pronounced, due to important changes in the horizontal ice sheet domain. Apart from the supposition that the ice sheet might have been somewhat smaller in the Ross embayment, this picture seems to fit well in Antarctic reconstructions based on empirical field evidence (e.g., Denton and Hughes 1981; Denton et al. 1989). It also indicates that the model is able to describe the relevant physics of the coupled ice sheet-ice shelf system in an essentially correct way.

The corresponding basal melting areas in these experiments are shown in Fig. 8. These fields are important in the dynamics of the ice sheet, as they constrain areas where basal sliding may occur. The occurrence of melting also indicates that old ice is gradually lost at the base and this is relevant to the establishment of a time scale for bottom layers in deep ice cores. As a general picture, higher ground below the EAIS seems to be largely unaffected by basal melting, that becomes nevertheless widespread when the ice sheet completely grounds under present *climatic* conditions (Fig. 8, 4). Besides thickening the ice, another effective way to warm the base then appears to reduce accumulation rates (Fig. 8, 2), so that less cold ice is advected downwards. It is also interesting to note that the ice sheet filling the Ross and Ronne-Filchner embayments at maximum glaciation is always wet-based.

Figure 9 summarizes the evolution of some large-scale model variables during these sensitivity runs. Shown are the number of grounded grid-points (1 grid-point represents an area of 16.10^8 m^2; Fig. 9, A) and ice volume expressed in equivalent sea level (Fig. 9, B), where allowance has been made for grounded ice merely displacing ocean water. Looking at model run (6), which is the glacial state (see explanation of Fig. 7), it appears that the ice sheet area has expanded by 17%, but the volume has increased from 25.0 to 32.4 10^6 km^3 of ice (i.e. +30%). This corresponds to an Antarctic contribution to global sea level lowering of some 16 m. Also, it appears that it may take up to 30–40000 years for the Ross and Ronne-Filchner ice shelves to become completely replaced by grounded ice. This is mainly a consequence of the low accumulation rates prevailing over the Antarctic ice sheet. Since environmental conditions have not been stable in the Antarctic for this length of time, it seems unlikely that a steady state description is really appropriate in reconstructing the ice sheet history during a complete glacial cycle. As demonstrated in Huybrechts (1990), these long time scales are also a likely explanation for the possible overprediction of ice sheet cover in the Ross sea.

Fig. 7. Steady state ice sheet geometries in response to glacial-interglacial changes in boundary conditions. Elevation contours (in km) are 0.5 km apart, the lowest contour is the grounding line. (*1*) interglacial reference run; (*2*) glacial accumulation rate (around 50–60% of Holocene values); (*3*) background temperature drop of 10° C; (*4*) global sea level depression by 130 m; (*5*) combination of 2 and 3; (*6*) full glacial conditions, i.e., a combination of 2, 3 and 4

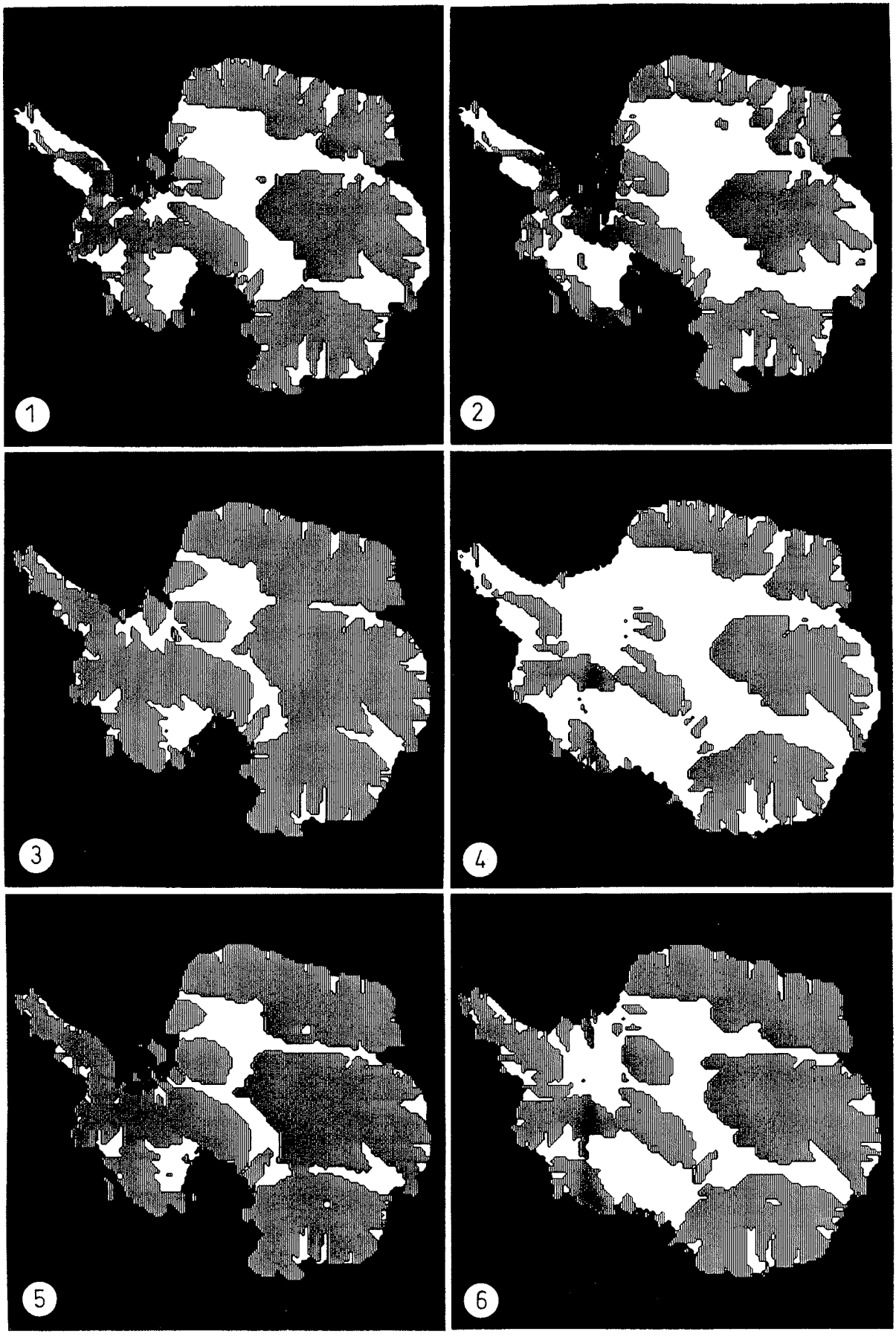
1
2
3
4
5
6

Concluding remarks

In this study, a rather comprehensive and detailed model for the entire Antarctic ice sheet was presented, designed for climatic change experiments. Although the formulation of some components of ice mechanics could certainly be improved as more accurate measurements become available (in particular: basal sliding and the stress balance at the grounding line), an important conclusion nevertheless seems to be that the model is apparently able to account for major characteristics of the Antarctic ice sheet, in present as well as past environments. As such, the model is certainly a useful tool in order to better understand and simulate the ice sheet in (palaeo-)climatic studies.

We examined the effects of glacial-interglacial changes in environmental conditions on its geometry. It turned out that most of the spreading of grounded ice across the shallow Ross and Weddell seas during glacial periods can be attributed to lower global sea levels. Lower ice temperatures also lead to expanded ice cover, but we found the associated reduced accumulation rates to largely counteract the effect. The role of sea level is particularly interesting, given the difficulties in reconciling the approximate simultaneity of glacial expansion in both hemispheres, with the Milankovitch forcing. It supports the hypothesis that the Antarctic ice sheet is basically linked to glacial evens on the northern hemisphere continents through changes in eustatic sea level. In the model, the most pronounced fluctuations occurred in the West Antarctic ice sheet geometry and the Ronne-Filchner ice shelf appeared to be more sensitive to grounding than the Ross ice shelf. On the East Antarctic plateau, on the other hand, resulting changes in surface elevation during a typical glacial-interglacial shift were generally within 100 m or so. This has wider implications, as it indicates that palaeoclimatic information derived from deep ice cores (Vostok, Dome C) have probably not been biased too much by level fluctuations and, hence, are likely to be essentially of climatic origin.

According to our reconstructions, a steady state Antarctic ice sheet may contribute some 16 m to global sea level lowering at maximum glaciation. However, due to the long-response time-scales involved, it is unlikely that the ice sheet ever reached a stationary state and this figure would even be reduced to 12 m if a complete glacial cycle is modelled (Huybrechts 1990). It is interesting to note that this figure is noticeably less than the 35 m put forward by Nakada and Lambeck (1987), who obtained this value as a residual by subtracting equivalent ice volume of fully grown northern hemisphere ice sheets from 130 m of sea-level. This discrepancy could imply that the northern hemisphere ice sheets have contained substantially more ice than assumed in their analysis, or, alternatively, sea level was depressed by less than 130 m.

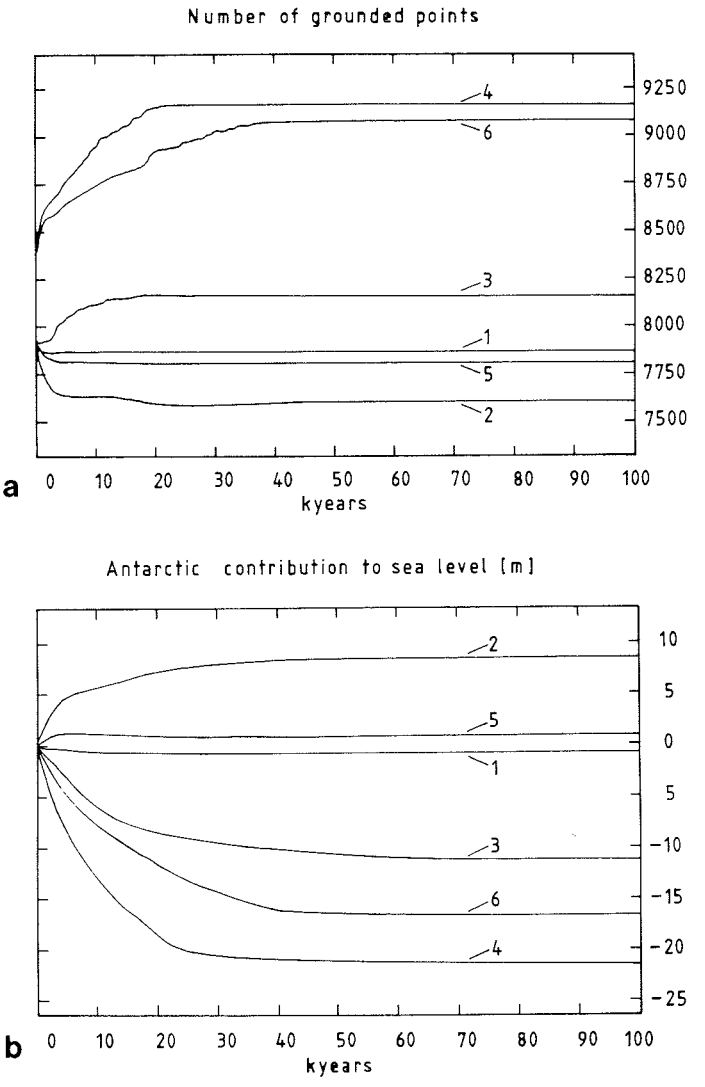

Fig. 9 A, B. Evolution of some large-scale model variables in the various simulations. In these experiments, a sudden stepwise alteration in boundary conditions is applied at time = 0. **A:** ice sheet area. **B:** grounded ice volume expressed in changes of global sea level. *Numbers* relate to the experiments in Fig. 7

Fig. 8. Basal ice sheet areas at pressure melting point (*white*) associated with the sensitivity experiments in Fig. 7. *Vertical shading* represents areas where the bed is frozen to the bedrock

Acknowledgements. This research would not have been possible without the support of the Alfred Wegener Institut, Bremerhaven, particularly for their CRAY-2 facilities and optimal working conditions provided during an 8-month stay. I would also like to express my thanks to Hans Oerlemans, who introduced me to the field of ice sheet modelling, and whose critical remarks were most valuable. Useful discussions with K. Herterich and J. Determann were also much appreciated. This work is part of the Belgian Program "Scientific Research on the Antarctic" (Services of the Prime Minister - Science Policy Office), while the author was supported by the Belgian National Fund for Scientific Research (NFWO).

References

Alley RB, Whillans LM (1984) Response of the East Antarctic ice sheet to sea-level rise. J Geophys Res 89 (C4):6487–6493

Bindschadler R (1983) The importance of pressurized subglacial water in separation and sliding at the glacier bed. J Glaciol 29 (101):3–19

Brotchie JF, Silvester R (1969) On crustal flexure. J Geophys Res 74 (22):5240–5252

Budd WF, Smith IN (1982) Large-scale numerical modelling of the Antarctic ice sheet. Ann Glaciol 3:42–49

Budd WF, Corry MJ, Jacka TH (1982) Results from the Amery Ice Shelf Project. Ann Glaciol 3:36–41

Budd WF, Jenssen D, Smith IN (1984) A three-dimensional time-dependent model of the West Antarctic ice sheet. Ann Glaciol 5:29–36

Budd WF, Jenssen D (1989) The dynamics of the Antarctic ice sheet. Ann Glaciol 12:16–22

Chapell J, Shackleton NJ (1986) Oxygen isotopes and sea level. Nature 324:137–140

Denton GH, Hughes TJ (1981) The last great ice sheets. John Wiley, New York

Denton GH, Bockheim JG, Wilson SC, Stuiver M (1989) Late Wisconsin and early Holocene glacial history, inner Ross embayment, Antarctica. Quat Res 31:151–182

Drewry DJ (1979) Late Wisconsin reconstruction for the Ross sea region, Antarctica. J Glaciol 24 (90):231–244

Drewry DJ (ed) (1983) Antarctic glaciological and geophysical folio. Scott Polar Research Institute, Cambridge

Elverhøi A (1981) Evidence for a late Wisconsin glaciation of the Wedell sea. Nature 293:641–642

Fortuin JPF, Oerlemans J (1990) Parameterization of the annual surface temperature and mass balance of Antarctica. Ann Glaciol 14:78–84

Greishar L, Bentley CR (1980) Isostatic equilibrium grounding line between the West Antarctic inland ice sheet and the Ross ice shelf. Nature 283:651–654

Herrod LDB (1986) Sea-bottom topography beneath Ronne ice shelf, Antarctica. Filchner Ronne ice shelf programme Report No 3, Bremerhaven, Alfred Wegener Institut, 72–80

Herterich K (1987) On the flow within the transition zone between ice sheet and ice shelf. In: Van der Veen CJ, Oerlemans J (eds) Dynamics of the West Antarctic ice sheet. D. Reidel, Dordrecht, pp 185–202

Herterich K (1988) A three-dimensional model of the Antarctic ice sheet. Ann Glaciol 11:32–35

Hutter K (1983) Theoretical glaciology. D. Reidel, Dordrecht

Huybrechts P (1986) A three-dimensional time-dependent numerical model for ploar ice sheets: some basic testing with a stable and efficient finite-difference scheme. Vrije Universiteit Brussel Geog Inst Report 86/1

Huybrechts P, Oerlemans J (1988) Evolution of the East Antarctic ice sheet: a numerical study of thermo-mechanical response patterns with changing climate. Ann Glaciol 11:52–59

Huybrechts P (1990) The Antarctic ice sheet during the last glacial-interglacial cycle: a three-dimensional experiment. Ann Glaciol 14:115–119

Huybrechts P, Oerlemans J (1990) Response of the Antarctic ice sheet to future greenhouse warming. Clim Dyn 5:93–102

Jenssen D (1977) A three-dimensional polar ice-sheet model. J Glaciol 18 (80):373–389

Jouzel J, Merlivat L (1984) Deuterium and Oxygen 18 in precipitation: modelling of the isotopic effects during snow formation. J Geophys Res 89 (D7):11749–11757

Jouzel J, Lorius C, Petit CR, Genthon C, Barkov NI, Kotlyakov VM, Petrov VM (1987) Vostok ice core: a continuous isotope temperature record over the last climatic cycle (160000 years). Nature 329:403–408

Jouzel J, Raisbeck G, Benoist JP, Yiou F, Lorius C, Raynaud D, Petit JR, Barkov NI, Korotkevich YS, Kotlyakov VM (1989) A comparison of deep Antarctic ice cores and their implicaton for climate between 65000 and 15000 years ago. Quat Res 31:135–150

Lorius C, Jouzel J, Ritz C, Merlivat L, Barkov NI, Korotkevich YS, Kotlyakov VM (1985) A 150000-year climatic record from Antarctic ice. Nature 316:591–596

McMeeking RM, Johnson RE (1985) On the analysis of longitudinal stress in glaciers. J Glaciol 31:293–302

Mitchell AR, Griffiths DF (1980) The finite difference method in partial differential equations. John Wiley, Chichester

Nakada M, Lambeck K (1988) The melting history of the late Pleistocene Antarctic ice sheet. Nature 333:36–40

Nye JF (1969) The effect of longitudinal stress on the shear stress at the base of an ice sheet. J Glaciol 8 (53):207–213

Oerlemans J (1982) A model of the Antarctic ice sheet. Nature 297:550–553

Oerlemans J, Van der Veen CJ (1984) Ice sheets and climate. D. Reidel, Dordrecht

Oswald GKA, Robin G de Q (1973) Lakes beneath the Antarctic ice sheet. Nature 245:251–254

Paterson WSB (1981) The physics of glaciers (2nd edn). Pergamon, Oxford

Robin G de Q (1977) Ice cores and climatic change. Phil Trans R Soc London B 280:143–168

Robin G de Q, Doake CSM, Kohnen H, Crabtree RD, Jordan SJ, Möller D (1983) Regime of the Filchner-Ronne ice shelves, Antarctica. Nature 302:582–586

Sclater JG, Jaupart C, Galson D (1980) The heat flow through oceanic and continental crust and the heat loss of the earth. Rev Geophys Space Phys 18:289–311

Shoemaker EM, Morland LW (1984) A glacier flow model incorporating longitudinal deviatoric stresses. J Glaciol 30 (106):334–340

Stuiver M, Denton GH, Hughes TJ, Fastook JL (1981) History of the marine ice sheet in West Antarctica during the last glaciation: a working hypothesis. In: Denton GH, Hughes TJ (eds) The last great ice sheets. John Wiley, New York, pp 319–436

Thomas RH (1973) The creep if ice shelves: theory. J Glaciol 12 (64):45–53

Thomas RH, MacAyeal DR, Eilers DH, Gaylord DR (1984) Glaciological studies on the Ross Ice Shelf, Antarctica, 1973–1978. In: Bentley CR, Hayes DE (eds) The Ross ice shelf: Glaciology and Geophysics. Antarctic Research Series 42:21–53

Turcotte DL, Schubert G (1982) Geodynamics. John Wiley, New York

Van der Veen CJ (1985) Response of a marine ice sheet to changes at the grounding line. Quat Res 24:257–267

Van der Veen CJ (1987) Longitudinal stresses and basal sliding: a comparative study. In: Van der Veen CJ, Oerlemans J (eds) Dynamics of the West Antarctic ice sheet. D. Reidel, Dordrecht, pp 223–248

Verbitsky MY (1988) Numerical experiments on the hydro-thermodynamics of the East Antarctic and Greenland ice sheets. In: Avsyuk GA (ed) Data of Glaciological studies, Chronicle discussions no. 40, Acad Sci USSR, 73–86

Weertman J (1964) The theory of glacier sliding. J Glaciol 5:287–303

Whillans IM, Chen YH, Van der Veen CJ, Hughes TJ (1989) Force budget: III. Application to three-dimensional flow of Byrd Glacier, Antarctica. J Glaciol 35 (119):68–80

Yiou F, Raisbeck GM, Bourles D, Lorius C, Barkov NI (1985) ^{10}Be in ice at Vostok, Antarctica during the last climatic cycle. Nature 316:616–617